STUDY ON THE EARTHQUAKE RESPONSE OF THE STRUCTURE-PILE-SOIL SYSTEM CONSIDERING LIQUEFACTION AND NON-LINEAR RESTORING FORCE CHARACTERISTICS OF SOIL LAYERS

Yoshihisa GYŌTEN(I), Koji MIZUHATA(I), Tadahiro FUKUSUMI(II)
Minoru FUKUI(III), Toshihiro ONO(IV)

SUMMARY

This paper presents the results of the earthquake response analysis of sandy soil layers and coupled soil-pile systems with and without rigid mass on the pile head, considering nonlinearity of the restoring force characteristics and the liquefaction of a saturated sandy soil layer as the reduction of shear modulus of soil. The lateral resistance factor obtained in the response analysis is compared with that obtained in the experiment referring to actual construction of piles in reclaimed sandy soil layers.

INTRODUCTION

It is one of the most serious problems in the earthquake resistant design to make the dynamic characteristics of soil layers clear. For these ten years the soil liquefaction as a remarkable critical phenomenon of soil has attracted attention and been studied (1), (2). This study reports the results of the dynamic response analysis of sandy soil layers, and coupled soil-pile systems with and without rigid mass on the pile head, considering the nonlinearity of the restoring force characteristics and the liquefaction of a saturated sandy soil layer as the reduction of shear modulus of soil. Further, the lateral resistance factor obtained in the response analysis is compared with that obtained in the experiment referring to actual construction of piles in reclaimed sandy soil layers.

EARTHQUAKE RESPONSE ANALYSIS OF SOIL LAYERS CONSIDERING LIQUEFACTION

Assumptions

In this analysis, the following assumptions are laid for soil characteristics.

(1) The restoring force characteristics of sandy soil is assumed to be of Hardin-Drnerich Masing type(3). The skelton curve is expressed as follows:

$$\tau = G_0\gamma/(1 + G_0\gamma/\tau_y) \tag{1}$$

where γ: shear strain, τ: shear stress, G_0: initial shear modulus, τ_y: maximum virgin shear stress. Eq.1 is normalized as Eq.2 by τ_y and the reference strain, γ_r, and the hysteresis loop can be expressed as Eq.3 by the Masing model.

$$\left(\frac{\tau}{\tau_y}\right) = \left(\frac{\gamma}{\gamma_r}\right)/\left(1 + \left|\frac{\gamma}{\gamma_r}\right|\right) \tag{2}$$

$$\left(\frac{\tau \pm \tau_0}{2\tau_y}\right) = \left(\frac{\gamma \pm \gamma_0}{2\gamma_y}\right)/\left(1 + \left|\frac{\gamma \pm \gamma_0}{2\gamma_y}\right|\right) \tag{3}$$

In Eqs. 1 and 3, τ_y can be obtained by Eq.4 and G_0 by Eq.5 as proposed by Richart.

$$\tau_y = [\{(1 + k_0)\sin\phi/2\}^2 - \{(1 - k_0)/2\}^2]^{1/2}\sigma_v \tag{4}$$

$$G_0 = 700\,\frac{(2.17 - e)^2}{1 + e}\left(\frac{1 + 2k_0}{3}\right)^{1/2}\sqrt{\sigma_v} \tag{5}$$

(I),(II): Professor, Research Associate, Kobe University, Japan
(III) : Nikken Sekkei Ltd. and Graduate Student, Kobe University, Japan
(IV) : Former Graduate Student, Kobe University, Japan

where k_o: coefficient of earth pressure at rest, e: void ratio, σ_v: vertical effective stress, ϕ: effective angle of shearing resistance.
(2) In the process of liquefaction, it is assumed that the stress-strain curve degrades step by step as Fig. 2, and the reduction of stiffness can be considered as the change of vertical effective stress, caused by the increase of excess pore-water pressure in Eqs.4 and 5. The dynamic equilibrium is considered in the continuation of stress and strain before and after the change of pore-water pressure.
(3) The incremental excess pore-water pressure is estimated as follows:
(a) It is estimated for every one cycle and for the average shear stress amplitude in the dynamic response analysis.
(b) From the S-N curves of sand for liquefaction ie. τ/σ_v vs. N_l by Tanimoto [4] as Fig. 4, the number of cycles for liquefaction N_l can be obtained.
(c) From the buildup curve of pore pressure proposed by Seed[1], i.e. γ_u vs. N/N_l as Fig. 3, the pore pressure ratio γ_u can be obtained.
(d) Further, the condition of initial liquefaction is made as follows: When the average shear stress ratio, τ/σ_v, equals to the dynamic effective angle of shearing resistance at a certain cycle, the liquefaction occurs.

Earthquake Response Analysis

Consider a stratum of saturaled sand having approximately uniform properties for lateral and vertical extent, resting on horizontal bedrock. The sand stratum is assumed to be shaken by horizontal shear waves. The sand stratum of 30m is divided into 10 layers. The water level under the ground is assumed to be GL-1.5m and GL-4.5m. As for the constants used in this analysis, it is assumed that the coefficient of earth pressure at rest, k_o, equals 0.5, and that the coefficient of pore pressure for the ascending curve by Seed, α, equals 0.7. The properties of sands are shown in Table 1 for Case-A, and Case-B, where the parameters are obtained from the laboratory tests by Tanimoto[4]. The differential equation of motion is written as

$$[Mi]\{\ddot{x}i\} + [Ci]\{\dot{x}i\} + [Ki]\{xi\} = - [Mi]\ddot{u}g(t) \qquad (6)$$

in which [Mi] is the diagonal mass matrix, [Ci] the viscous damping matrix, $\ddot{u}g(t)$ the earthquake acceleration at the base of the layer. $\{xi\}$, $\{\dot{x}i\}$, and $\{\ddot{x}i\}$ are displacement, velocity, acceleration of the mass [Mi] relative to the base, respectively, the viscous damping being propotional to the initial shear modulus equivalent to 5% of critical damping in this analysis. The input earthquake recorded at Kobe Port Island (P.I.) in Japan, Taft, and El-Centro of different maximum amplitudes are used. Eq.6 is integrated by the Runge Kutta's Method, where time step is 0.01 sec.

Results and Discussions

The natural periods of the analyzed soil deposits for the initial shear modulus are 0.47 sec. for Case-A, 0.52 sec. for Case-B. The distributions of pore pressure response with depth are shown in Figs. 5(a) ∿ 5(d), in which, the pore pressure is divided by the initial vertical effective stress, and presented by γ_u. If γ_u equals to 1.0, liquefaction occurs in the respective layer. In all of the analyzed cases, the layers liquefied were from GL-6.0m to GL-12.0m, and it becomes clear that at several meters below the water table, liquefaction occurred most easily, because the ratio τ/σ_v becomes larger, while in the layers under the depth of GL-15.0m, liquefaction did not occur. In the following, the effects of the combination of parameters used in this analysis are discussed.

First, the effect of input acceleration is discussed. As shown in Fig. 5(a) liquefaction occurs at t=6.0 sec. for the input acc. of P.I. wave whose

max. is 100 gal., but as shown in Fig. 5(b) it occurs at t=14.5 sec. for the input acc. of Taft wave whose max. is 200 gal. For the input acceleration of Taft whose max. is 100 gal., liquefaction doesn't occur. Then, it is stated that possibility of liquefaction depends on the characteristics of the earthquake wave.

Second, the effect of soil deposit is discussed. As shown in Fig. 5(a) and Fig. 5(b), liquefaction occurs at t=6.0 sec. for Case A and at t=4.0 sec. for Case-B, this mainly reflects the S-N curves (Fig. 4).

Finally, the effect of the depth of the water level is discussed. As shown in Figs. 5(a) and (d), liquefaction occurs in the case of the water level of GL-1.5m, but it doesn't occur in the case of the water level of GL-4.5m. The relation of force vs. displacement on GL-9.0m in Fig. 5(a) is shown in Fig. 6, where the input acceleration is P.I. wave, whose max. is 100 gal. In Fig. 6, (a) denotes the case of neglecting liquefaction, and (b) denotes the case of considering it. Figs. 8 and 9 show the responses of shear stress and shear strain, respectively, for P.I. wave, whose max. is 100 gal. After the moment of liquefaction, the shear stress was not transmitted upward, and the shear strain became larger and drifted on one side. Fig. 10 shows the acceleration response on the ground surface. In Fig. 10, the solid line is for the case of considering liquefaction, while the dotted line is for the case of neglecting liquefaction. Comparing the solid line with the dotted one, one notices that the amplitude of response acceleration is small before and after the liquefaction, and that the periodic characteristics is changed after liquefaction.

EARTHQUAKE RESPONSE ANALYSIS OF SOIL-PILE SYSTEM

Method of Analysis

The method of dynamic response analysis follows the Penzien's procedure (5), which may be one of general and basic procedures for the dynamic problem of lumped-mass soil-pile systems. The differential equation of motion of the soil-pile system is,

$$[Mi^P]\{\ddot{X}i\} + [Cij^P]\{\dot{X}i\} + [Kij^P]\{Xi\} + [Mi^e]\{\ddot{X}i - \ddot{x}i\} + [Ci^e]\{\dot{X}i - \dot{x}i\} + [Ki^e]\{Xi - xi\} = -[Mi^P]\ddot{u}g(t) \qquad (7)$$

in which, $[Mi^P]$, $[CijP]$ and $[KijP]$ are the mass matrix, the viscous damping matrix, the stiffness matrix of pile, respectively; $[Mi^e]$, $[Ci^e]$ and $[Ki^e]$ are the effective mass matrix, the effective viscous damping matrix, the effective horizontal spring matrix of soil-pile interaction, respectively; $\{Xi\}$, $\{\dot{X}i\}$ and $\{\ddot{X}i\}$ are displacement, velocity, acceleration of the pile, respectively, and $\{xi\}$, $\{\dot{x}i\}$, and $\{\ddot{x}i\}$ are displacement, velocity, acceleration of the soil determined by Eq.6. In Eq.7, the horizontal spring, the effective mass of the soil are calculated after Mindlin. In this study, the single pile with mass on its head is analyzed. The pile is a steel pipe pile of 10mm thick and 600mm in diameter, the mass on the pile head is taken to be five times as large as that of the pile, the length of the pile is 21 meters, and the pile is divided into seven lumped masses. As for the boundary condition of the pile, it is assumed that the pile head is slidingly fixed and the pile tip is fixed. For considering the nonlinearity of soil, the horizontal spring constants are calculated for three cases shown in Table 2. The values of the horizontal spring constant per unit length and the effective mass used in this analysis are shown in Fig. 13 and 14. The horizontal spring constants are considered to be propotional to reduction of soil stiffness. The input earthquake acceleration is that of P.I. wave whose max. is 100 gal. as before, and the differential equation, Eq.7, is

integrated by the Runge Kutta's method where time step is 0.01 sec.

Results and Discussions

The excess pore water pressure response is shown in Fig. 15. As shown in Fig. 15, only the 6th layer liquefied at t≒5.5 sec. In Fig. 16, the solid line shows the displacement responses at the pile head, and the dotted line shows that on the surface of soil. It is noticed from Fig. 16, that the displacement of pile head is almost the same as that of soil, because of restraint of the upper soil layer near the surface whose stiffness is not so much reduced. The shape of the displacement response of the pile and the soil is shown in Fig. 17 with 2.0 sec. interval where the solid line is that of the pile and the dotted one is that of the soil. The pile is forced to displace larger on 4th and 5th layers than on others. Further, the maximum bending moments appeared in the analysis for three cases are shown in Fig. 18. As for Case-1, where the horizontal spring constant is not so large as those of the others, it is not so clear, but as for Case-2 and Case-3, it is clear that the bending moment of the pile becomes larger in the liquefied sandy layer than that in the other layers. The acceleration response of the pile head is shown in Fig. 19, where (a) denotes neglecting liquefaction and (b) denotes considering liquefaction. It is recognized from Fig. 19 that the higher frequency predominates in the process of soil liquefaction, particularly after the soil liquefaction. It seems that predominant higher frequency components in the acceleration response is caused by the phase lag between the input acceleration and the response acceleration of the soil transmitted through the effective mass of soil, and the difference of displacement between the pile and the soil transmitted through the horizontal spring. Fig. 20 shows the relation between the shear force of the pile, $[K^{P}ij]\{Xi\}$, and the relative displacement of soil and pile, $\{Xi - xi\}$, at the pile top for the earthquake response analysis in Case 1 of Table 2. It is recognized in Fig. 20 that the shear force of the pile at the top increases catastrophically at the beginning of liquefaction and after that the shear force displacement curve varies complicatedly, and the shear force decreases. The horizontal spring constants at the pile top before liquefaction are about 18.5 ∿ 34.0 t/cm for Case 1 (Go/10) ∿ Case 3 ($G_O/2$) and these values do not change so much after liquefaction. This may be because the liquefied portion is limited in narrow range, compared with the total length of the pile, and it does not influence so much on the horizontal spring constant at the pile top.

EXPERIMENTAL VALUES OF LATERAL RESISTANCE UNDER ACTUAL CONDITIONS

In this section, the horizontal spring constant at the pile top calculated in the earthquake response analysis in last section is compared with that obtained in the experiment under actual construction conditions of piles in the reclaimed sandy layer. Under actual construction conditions in the reclaimed area, an earth auger is used in order to reduce the number of blows and to remove obstacles in the soil, and also, the reduced negative skin friction piles are often used, where the pile with enlarged point is effective in order to prevent the slip layer torn off and to increase the point bearing capacity. In both uses of the enlarged point and the earth auger, the clearance appears between the pile and soil, or the surrounding soil get loosen, and the lateral resistance properties of piles become worse compared with the usual cases.

Then, the authors conducted the following experiment in four sites in

the reclaimed area as shown in Fig. 21. Properties and dimensions of the piles used in the experiment are shown in Table 3 and Fig. 21. The test procedures are drawm in Fig. 22. As for piles T_1, T_2 and T_3, after driving without earth auger the clearance of about 5cm between the pile and soil was filled up with the site soil (for T_1) or cement milk (for T_2 and T_3). Before and after filling up the clearance, the static lateral loading tests and both the free and the forced vibration tests were conducted. For pile P_1 driven after boring 11m in depth by the earth auger of 700mm in diameter, the clearance of about 5cm was filled up with sand after driving. Pile S_1 was driven after excavation and boring 4m in depth by the earth auger of 700mm in diameter without filling up. Piles T_4 and T_5 were driven after boring 4m in depth by the earth auger of 600mm in diameter. As for pile T_4 after pile driving the clearance of about 5cm between the pile and soil was filled with sand, while as for pile T_5 the clearance was filled with sand during pile driving.

In the static lateral loading test, the horizontal force and displacement at the pile top were measured, and the horizontal spring constant, K_p, at the pile top was calculated. These results have been plotted in Figs. 23(a) and (b). Also, the lateral resistance factor, K_h, was calculated by Chang's formula and plotted against the displacement at the pile top in Fig. 24. In the free vibration test, the natural frequency and the damping factor were read from the displacement amplitude obtained by double integration of the record of the accelerometer. In the forced vibration test, a vibration generator set up on the rigid mass of concrete of 1.20 x 1.20 x 1.00m fixed on the pile head was operated by changing the frequency continuously from 0 to 12 Hz. The displacement of the rigid mass obtained by double integration of the record of the accelerometer set up on the rigid mass was plotted against the frequency and the resonance frequency and the damping factor were read out. The results of the free and the forced vibration tests are shown in Table 4. From Figs. 23 and 24 and Table 4, the following have been mentioned: The lateral resistance factor increases very much by filling up the clesrance between the pile and soil. The largest increase of the lateral resistance can be obtained by filling with selected sand after pile driving (T_4), and the smallest one is obtained by filling with site soil after pile driving (T_1). The intermediate one is obtained by filling with cement milk after pile driving (T_2, T_3) as well as with selected sand during pile driving (T_5). The natural frequencies in the free vibration tests are well correlated to the lateral resistant factor in the static test near the displacement of 2mm for piles T_2 and T_3 by the Chang's assumption.

CONCLUSIONS

The following are concluded in the above-mentioned study:
(1) Liquefaction tends to occur most easily at several meters deep under the water table, and the possibility of liquefaction depends on the characteristics of the input earthquake acceleration and it becomes lower as the water level becomes deeper.
(2) As for the response of soil, on the ground surface, the displacement becomes larger, the acceleration amplitude decreases, and the frequency characteristics is changed due to liquefaction of the middle layer.
(3) As for the response of the soil-Pile system, the bending moment of the pile becomes larger in the liquefied layer, and in the acceleration response of the pile the higher frequency predominates after liquefaction. The shear force of the pile at the top increases catastrophically at the beginning of

liquefaction and after that the shear force displacement curve at the pile top varies complicatedly. The horizontal spring constant at the pile top does not change so much before and after liquefaction.
(4) The effect of filling up the clearance between the pile and soil on the lateral resistance of the pile increases in the following order: Site soil after pile driving < Cement milk after pile driving ≦ Selected sand during pile driving < Selected sand after pile driving.
(5) The horizontal spring constants of 18.5 t/cm ∿ 34 t/cm obtained in the earthquake response analysis drop in the range of those obtained in the experiment for the same amount of displacement.

Table-1 Soil Properties used in the Analysis

	Case-A			Case-B		
Depth (m)	G (kg/cm)	τy (kg/cm²)	Para-meter	G (kg/cm)	τy (kg/cm²)	Para-meter
1.5	1.658	0.114		1.258	0.100	
4.5	2.345	0.228	ρ:1.9 (g/cm³)	1.780	0.200	ρ:1.8 (g/cm³)
7.5	2.872	0.342		2.180	0.299	
10.5	3.317	0.456		2.517	0.399	
13.5	3.708	0.570	e:0.57	2.814	0.499	e:0.7
16.5	4.062	0.685		3.082	0.599	
19.5	4.388	0.799	φ: 39.0	3.328	0.698	φ: 36.5
22.5	4.691	0.913		3.558	0.798	
25.5	4.975	1.027	φ': 33.0	3.775	0.898	φ' 30.0
28.5	5.244	1.141		3.979	0.998	

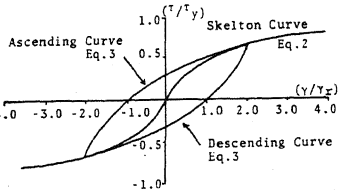

Fig.1 Normarized Hardin-Drnevich Masing Model

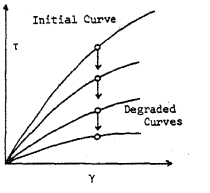

Fig.2 Degrading of Skelton Curve

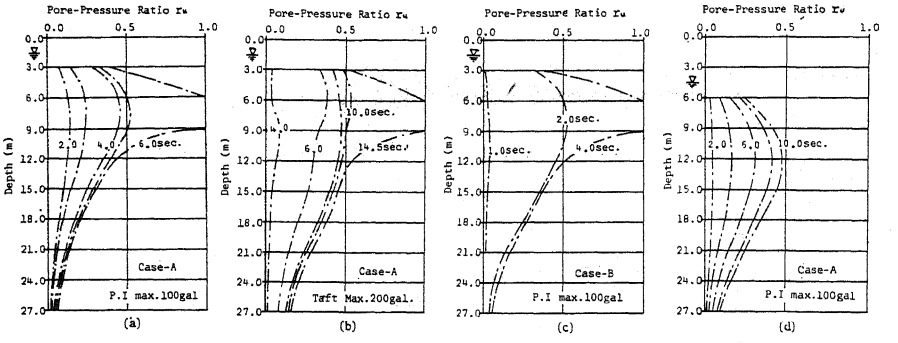

Fig.5 Pore Pressure Distribution with Depth During Earthquakes

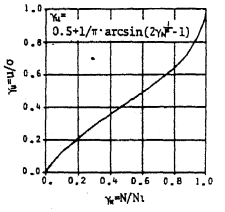

Fig.3 Rate of Pore Pressure Buildup (by Seed)

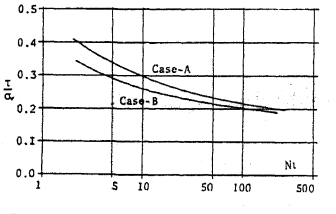

Fig.4 S-N Curves of Sandy Soil for Liquefaction (by Tanimoto)

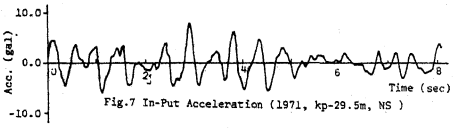

Fig.7 In-Put Acceleration (1971, kp-29.5m, NS)

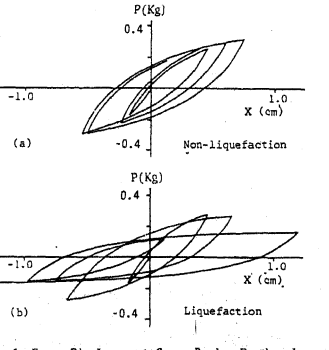

Fig.6 Force-Displacement Curve During Earthquake

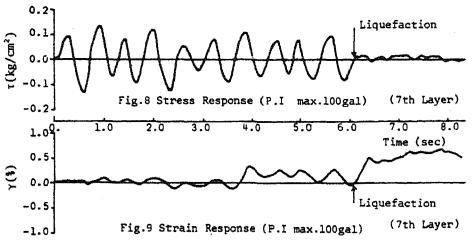

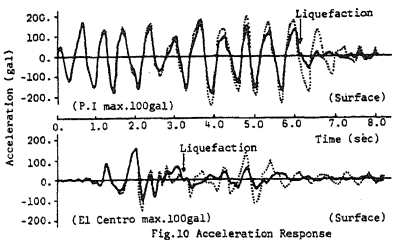

Fig.10 Acceleration Response

Table-2 Horizontal Interaction Spring in the Analysis

Case-1	1/10Go
Case-2	1/4Go
Case-3	1/2Go

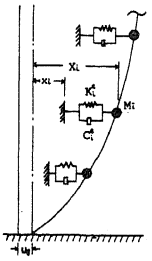
Fig.11 Penzien Model of Soil-Pile System

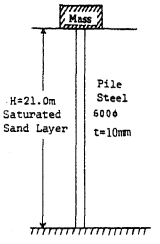

Fig.12 Analized Model

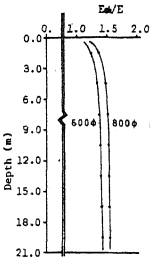

Fig.13 Horizontal Spring Constant per Unit Length

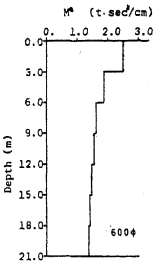

Fig.14 Effective Mass

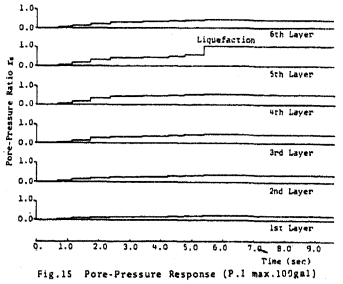

Fig.15 Pore-Pressure Response (P.I max.100gal)

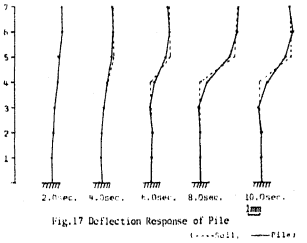
Fig.17 Deflection Response of Pile

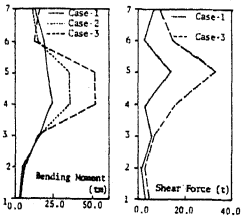

Fig.18 Maximum Bending Moment and Shear Force Response of the Pile

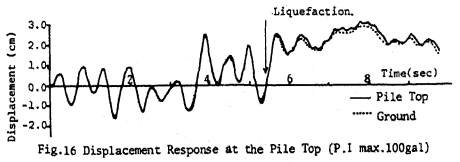

Fig.16 Displacement Response at the Pile Top (P.I max.100gal)

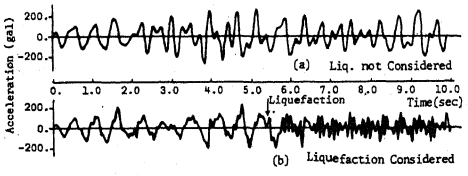

Fig.19 Acceleration Response at the Pile Top (P.I max.100gal,Case-2)

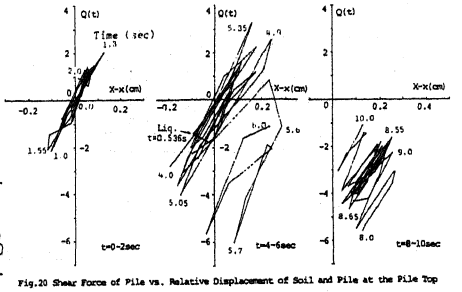

Fig.20 Shear Force of Pile vs. Relative Displacement of Soil and Pile at the Pile Top (Case-1 P.I Max.100gal)

Table-3 Properties and Dimensions of Pile

Site	Pile	Pile Material	Upper Part			Lower Part		Earth Auger		Filled Material
			ϕ_U	t_U	L_U	ϕ_L	L_L	ϕ_E	L_E	
A	T1	Steel	600	12.7	14.3	700	5.0	(not used)		Site Soil
	T2	Steel	600	12.7	14.3	700	5.0	(not used)		Cement Milk
	T3	Concrete	600	100.0	14.3	700	5.0	(not used)		Cement milk
B	P1	Concrete	500	90.0	27.0	600	6.0	600	11.0	Sand
C	S1	Steel	660	12.7	38.9	(Straight)		700	4.0	(None)
D	T4	Steel	500	12.0	26.5	600	6.0	600	4.0	Sand
	T5	Steel	500	12.0	26.5	600	6.0	600	4.0	Sand

ϕ(mm) and L(m) : Diameter and Length of Pile or Earth Auger
t(mm) : Thickness of Upper Portion of Pile

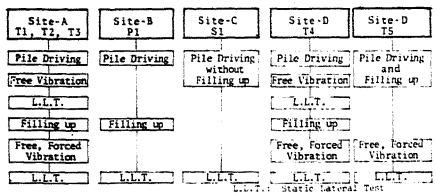

Fig.22 Test Procedure

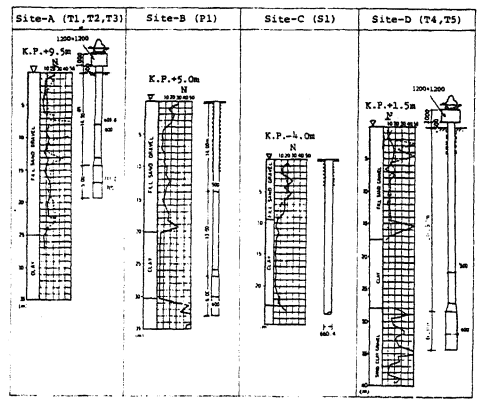

Fig.21 Profiles of Soil and Piles

Table-4 Free and Forced Vibration Test Results

Pile	Test	Free Vibration Test: Natural Frequency f (c/s)	Free Vibration Test: Damping Factor	Forced Vibration Test: Resonance Frequency f (c/s)	Forced Vibration Test: Damping Factor
T1	B*	5.7	0.11	——	——
	A*	7.3	0.14	5.0	0.12
T2	B*	5.6	0.10	——	——
	A*	12.1	0.10	6.5	0.15
T3	B*	5.1	0.12	——	——
	A*	16.2	0.09	——	——
T4	B*	4.2	0.04	(f_{re}>5.5)*	——
	A*	6.1	0.12	(f_{re}>5.5)*	——
T5	A*	9.2	0.07	(f_{re}>5.5)*	——

B* and A* : Vibration Test Before and After Filling up
(f_{re}>5.5)*: Test Frequency was less than Resonance Frequency, f_{re}

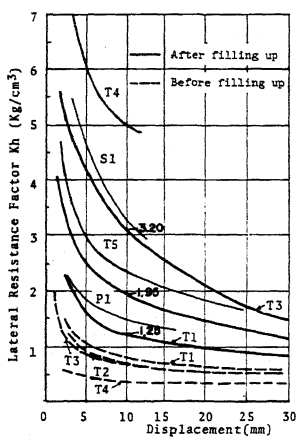

Fig.24 Relation of Lateral Resistance Factor vs. Displacement

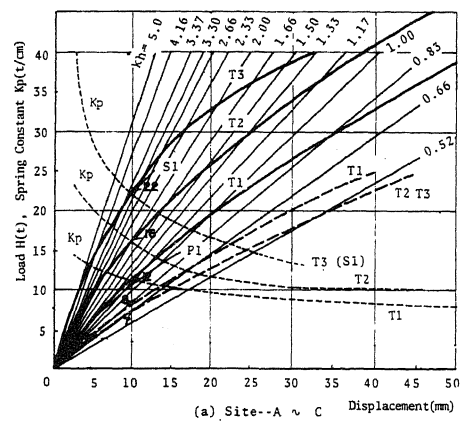

(a) Site--A ∿ C

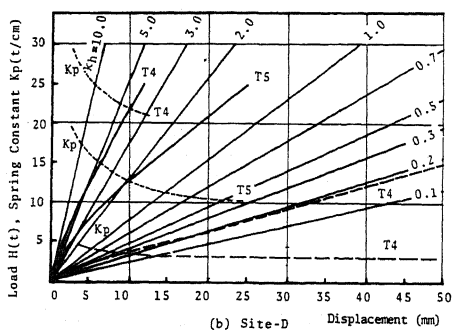

(b) Site-D

Fig.23 Load and Spring Constant vs. Displacement
(----Before Filling, ——After Filling)

REFERENCES

(1) Seed,H.B., "Pore-Water Pressure Changes during Soil Liquefaction" J.S.M.F.D. Proc.ASCE Vol.102 No. GT4 pp.323-346 (1976)
(2) Finn,W.D.L., Lee,K.W. and Martin,G.R.,"Dynamic Effective Stress Analysis of Sand" Proc. 9th I.C.S.M.F.E. Vol.2 pp.231-236 (1977)
(3) Hardin,B.O. and Drnevich,V.P., "Shear Modulus and Damping in Soils Design Equations and Curves" J.S.M.F.D. Proc. ASCE Vol.98 No. SM7 pp.667-692 (1972)
(4) Tanimoto,K. and Uemura,T.,"Failure of Saturated Sands under Cyclic Loading" Proc.of J.S.C.E. Vol.183 pp.63-71 (1970)
(5) Penzien,J., Sheffy,C. and Parmelee,R., "Seismic Analysis of Bridges on Long Piles" J.E.M.D. ASCE Vol.90 No. EM4 pp.41-68 (1965)